ASME Journal of Energy Resources Technology
Online journal at:
https://asmedigitalcollection.asme.org/energyresources

Potential Impacts of Climate Change on Renewable Energy and Storage Requirements for Grid Reliability and Resource Adequacy

Clifford K. Ho[1]
Fellow ASME
Sandia National Laboratories,
P. O. Box 5800,
Albuquerque, NM 87111
e-mail: ckho@sandia.gov

Erika L. Roesler
Sandia National Laboratories,
P. O. Box 5800,
Albuquerque, NM 87185
e-mail: elroesl@sandia.gov

Tu Nguyen
Sandia National Laboratories,
P. O. Box 5800,
Albuquerque, NM 87185
e-mail: tunguy@sandia.gov

James Ellison
Sandia National Laboratories,
P. O. Box 5800,
Albuquerque, NM 87185
e-mail: jfellison@gmail.com

This paper provides a study of the potential impacts of climate change on intermittent renewable energy resources and storage requirements for grid reliability and resource adequacy. Climate change models and available regional data were first evaluated to determine uncertainty and potential changes in solar irradiance, temperature, and wind speed within a specific U.S. southwest service area as a case study. These changes were then implemented in solar and wind energy models to determine impacts on renewable energy resources. Results for the extreme climate change scenario show that the projected wind power may decrease by ~13% due to projected decreases in wind speed. Projected solar power may decrease by ~4% due to decreases in irradiance and increases in temperature. Uncertainty in these climate-induced changes in wind and solar resources was accommodated in probabilistic models assuming uniform distributions in the annual reductions in solar and wind resources. Uncertainty in battery storage performance was also evaluated based on increased temperature, capacity fade, and degradation in round-trip efficiency. The hourly energy balance among electrical load, generation, and storage was calculated throughout the year. The annual loss of load expectation (LOLE) was found to increase from ~0 days/year to a median value of ~2 days/year due to potential reductions in renewable energy resources caused by climate change and decreased battery performance. Significantly increased battery storage was required to reduce the LOLE to desired values of 0.2 days/year. [DOI: 10.1115/1.4062891]

Keywords: climate change modeling, solar resource, wind resource, capacity fade, resource adequacy, integrated resource plan, energy storage systems, renewable energy

1 Introduction

The potential adverse impacts of climate change have received significant attention over the last decade. Studies of the impact of climate and environmental changes on the performance of renewable energy systems, however, have significant gaps and tend to lack quantitative assessments regarding specific geographic regions [1–3]. A number of studies have evaluated the dependence of local ambient environmental parameters on energy performance [4,5], and novel methods such as incorporating machine learning to forecast and accommodate variability of local weather on demand-side management have been performed [6]. Wind-farm layout optimization using different multi-stage methods and local wind complexity has also been performed [7]. However, long-term impacts of climate change are generally neglected. Harang et al. [8] evaluated the impacts of climate change on energy demand due and loss of load expectation (LOLE) in Europe. They generally found that warmer temperatures in the winter will reduce energy demand overall in Europe, but they only considered the impacts of climate change on water inflows for hydropower. They did not investigate the impacts of climate change on solar and wind resources. The differentiating purpose of this study is to demonstrate and evaluate the potential impacts of climate change on future resource adequacy (solar, wind, and storage) with consideration of uncertainties in renewable energy resources and battery storage performance using regional climate data and resources in New Mexico as a case study.

In January 2021, the Public Service Company of New Mexico (PNM) issued its fifth Integrated Resource Plan (IRP), "PNM 2020–2040 Integrated Resource Plan," which included carbon-free electricity generation portfolios by 2040 [9]. PNM is a regulated utility and NM's largest energy provider with currently over 500,000 residential and business customers and ~3 GW of generation capacity. The PNM 2020-2040 IRP included portfolios to meet NM's Energy Transition Act, which requires 100% of electricity generation to be carbon free by 2045. PNM intends to meet that

[1]Corresponding author.

Contributed by the Advanced Energy Systems Division of ASME for publication in the Journal of Energy Resources Technology. Manuscript received February 19, 2023; final manuscript received June 24, 2023; published online July 24, 2023. Assoc. Editor: Hamidreza Najafi.

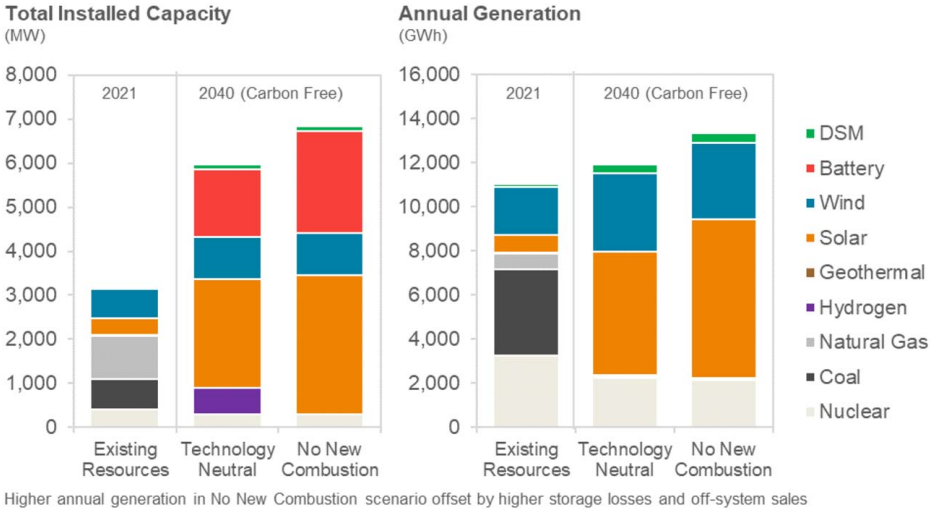

Fig. 1 PNM Portfolios for carbon-free electricity production in 2040 [9]

goal by 2040 and includes two different portfolios: a Technology Neutral scenario that includes hydrogen combustion turbines (initially powered by natural gas through the 2020 s), and a No New Combustion scenario that relies primarily on solar, wind, and battery storage (Fig. 1).

In the PNM 2020-2040 IRP, treatment of uncertainty and sensitivity analyses focused primarily on demand-side uncertainty. Climate change and potential impacts on intermittent wind and solar resources were not considered. In addition, uncertainties in large scale, long-term performance and reliability of battery storage systems were not considered; the battery storage system was assumed to operate at nameplate capacity for its entire 20-year lifetime (due to contracted maintenance and servicing of the systems).

The objectives of this study were to develop a probabilistic model and framework to evaluate inherent uncertainties in the energy resources and storage assumed in the PNM 2020-2040 IRP:

- Long-term changes in solar and wind resources caused by climate change.
- Uncertainties in battery performance caused by capacity fade, degradation in round-trip efficiency, and long-term temperature increase caused by climate change.
- Impact on the annual LOLE and required energy storage.

Probabilistic models were developed to evaluate the hourly energy balance each year given uncertainties in renewable energy resources and energy storage. The LOLE was probabilistically evaluated for the 2040 No New Combustion portfolio considering potential reductions in renewable energy resources and battery storage. The efficiencies and performance of renewable conversion systems (including batteries) and loads from heating, ventilation, and cooling (HVAC) systems were taken from current literature as a conservative estimate of overall performance.

2 Climate Change Modeling

2.1 Climate Data Source and Methods. Three simulations from the Department of Energy's Energy Exascale Earth System Model (E3SM) were chosen from the Earth System Grid Federation Climate Model Intercomparison Project—version 6 (CMIP6) repository [10–13]. The CMPI6 simulation set contains output contributed from earth system modeling centers. This set includes simulations representing the earth system response under various, prescribed forcing scenarios. For this study, the three simulations chosen were a baseline simulation called preindustrial control (piControl), a moderately warming simulation called historical, and a highly warming simulation called SSP585. The three simulations were from the "r1i1p1f1" variant identification, meaning the first realization, first initialization, and same physics and forcing. The data were all written in the form of monthly averages with more details below.

The baseline simulations include prescribed greenhouse gas concentrations, such as CO_2, set to values at a time in human history where anthropogenic signatures were not distinguishable by the temperature of the atmosphere. These baseline simulations start in the year 1850 and usually run with that concurrent year, 1850, for several hundred years. The purpose of the duration of these simulations is to emulate the earth system climate variability and seasonality so that statistically significant values for a baseline, unperturbed earth, can be compared against a simulated earth with increasing anthropogenic signatures such as increasing greenhouse gas concentrations. Table 1 lists the description of data used for the Preindustrial control, baseline data. Because this data set has no induced warming on the earth system, it was also referred to as the "no climate change" scenario for this work.

The historical simulation data set, also described in Table 1, uses CO_2 concentrations prescribed or calculated from years 1850 to 2014. The earth system will be warming due to increased greenhouse gas concentration build-up over this time period, so this data set was referred to as the "low climate change" scenario. The last simulation data set used is called SSP585. It was developed as an update of the high-emission "business as usual" IPCC RCP8.5 scenario [10,13]. This data set has the highest amount of warming of the three and is called "high climate change" in this work.

Table 1 Description of data sources from simulations used for three climate change scenarios over New Mexico

Scenario	Data and simulation description
No climate change	– Economics of climate adaptation (ECA) version of Preindustrial control simulation – CR-1.7 CMIP-6.2, ScenarioMIP – Concurrent year 1850 year for 165 years, monthly averages
Low climate change	– Update of RCP8.5 based on SSP5 – CR-1.7 CMIP-6.2, ScenarioMIP – Jan 1850–Dec 2014, monthly averages
Extreme climate change	– Update of RCP8.5 based on SSP5 – CR-1.7 CMIP-6.2, ScenarioMIP – 1032 monthly-averaged time points, Jan 2015–Dec 2021

Table 2 List of Variables for used to determine resources uncertainty for solar, wind, and battery

CMIP6 variable	Renewable resource	Description
sfcWind (m s^{-1})	Wind power	Near-surface (usually, 10 meters) wind speed in Time, (Latitude, Longitude) (1 deg) (180, 360)
rsds (W m^{-2})	Solar power	Surface Downwelling Shortwave Radiation in Time, (Latitude, Longitude) (1 deg) (180, 360)
Ts (K)	Solar power, Battery storage	Surface Temperature in Time, (Latitude, Longitude) (1_deg) (180, 360)

The variables chosen for analysis are fundamental variables influencing wind energy production, solar energy production, and battery storage efficiency. Table 2 lists the variables chosen from the E3SM CMIP6 database. For wind power generation, power is a function of wind speed cubed. The variable for near-surface wind, sfcWind, was used instead of wind at hub height. "sfcWind" is stated to be the wind at about 10 meters off the ground surface. It should be noted that the wind speed within the boundary layer generally follows a log wind profile as the surface frictional effects are less impactful as you move away from the surface. Therefore, any additional low-level increase in height—10 s to 100 s of meters will give "generally" an increase in wind speed and therefore power. This variable was readily available and required no additional data processing after downloading.

Solar energy production from solar installations relies on direct and diffuse solar radiation. The potential for solar energy production is computed from the Global Horizontal Irradiance (GHI), which is the sum of Diffuse Horizontal Irradiance (DHI) and Direct Normal Irradiance (DNI) multiplied by the cosine of the solar zenith angle (z), $GHI = DHI + DNI \cdot \cos(z)$. Given radiation parameterizations in earth system models are column-based physics with no radiation interaction between columns, the surface downwelling shortwave radiation is associated with the needed GHI variable. Clear-sky shortwave radiation at the surface from climate models is DNI, but the diffuse radiation that could be scattered equally in all directions from molecules, aerosols, and clouds is more difficult to ascertain from the earth system model output. Ground reflectance could also be included in GHI, but this contribution is usually low compared to DHI and DNI. It was determined that the variable "rsds" would be the most appropriate choice for determining solar variability with a changing climate.

The time-averaged global annual mean of the three simulations and the variables of interest give a notional sense of the global variability and magnitudes of the three variables, showing differences in energy, temperature, and wind over New Mexico compared to other regions of the globe. Qualitatively, there is little spatial difference between the "No Climate Change" and "Low Climate Change" scenarios. The "High Climate Change" scenario shows significant warming in the Arctic and in New Mexico. Wind speeds and surface downwelling shortwave radiation over New Mexico do not change as much as temperature across the three scenarios.

The time series trends for each of the variables for each of the simulation is shown in Fig. 2. The simulation output is in the form of monthly means, and a 48-point running average was computed for each of the time series. Three area-weighted averages were computed for comparison: the entire globe, the contiguous United States (i.e., lower 48 States), and the State of New Mexico. In the "No Climate Change" scenario, it is expected there to be little-to-no-trend over the time series because the earth system is in preindustrial energy equilibrium. The "Low Climate Change" scenario shows increasing surface temperatures in the latter portion of the simulation, which is consistent with observations and the basis upon which this simulation is designed. The trends in the surface downwelling shortwave radiation and near-surface wind speed also show minute changes at the end of the simulation. Impacts in the simulation of coarse spatial resolution and parameterizations, or not enough forcing to cause a discernable change in the time series, are all probably causes for these two variables' trends. The "High Climate Change" scenario shows the expected increase in surface temperature, a reduction in near-surface wind speed, and no discernable change in the surface downwelling shortwave radiation. There is little confidence in the trends of wind and radiation for this scenario (see Sec. 2.3).

2.2 Climate Modeling Results. Bounds and trends are needed for the solar and wind resource calculations. Because climate models are inherently uncertain in that they represent chaotic systems with much dependence on initial conditions for solutions, it was decided to take averages of the three simulations over the state of New Mexico. New Mexico's land area is small compared to the global surface, and instances of the climate over New Mexico for any given month could be representative of the past, current, and future climate. Table 3 shows the time averages and standard deviations over New Mexico for the entire simulations for the three variables.

From Table 3, there is no trend in surface downwelling shortwave radiation (i.e., solar radiation) over the "No," "Low," and "High" climate change scenarios. The variation in surface downwelling shortwave radiation might be due to the difference in time series plotted, where the "Low Climate Change" scenario is nearly twice as long as the "High Climate Change" scenario. The variation might also be due to the way the climate system manifests in models under different forcing scenarios. It is unknown if a future climate with average higher temperatures and greenhouse gases will have more or less variability compared to the current record of our climate system over the past 150 years. The near-surface wind decreases slightly from "No" to "High" climate change scenarios, and the temperature increases by 5 K from "No" to "High" climate change.

2.3 Comparison With Other Studies. This study is not alone in assessing climate change impacts on renewable energy resources. Global, national, and regional bodies of research exist for specific technologies as well as system-level studies. For future reference, Solaun and Cerdá [1] provide global overviews of climate change effects on renewable resources. Additionally, a nationwide assessment of energy demand under different emissions scenarios stated that electricity demand will increase by on average of 10%, which included power system generation with power system planning and operations [14]. In the literature review performed for this study, it was found that there is unanimous uncertainty in the magnitude and direction of energy resources being impacted regionally and under different future climate scenarios. The focus now narrows to literature that has the most direct application or comparison with this work; this section provides an overview of select literature reporting for the southwestern United States. For neighboring state Texas for solar and wind, the wind increases by 1–4%, but there is no clear concurrence on solar production for future years 2041–2050 [15,16].

Wind power, although very specific to the region, shows both an increase and decrease in potential wind energy production through the variability of wind speed projections over different seasons and emissions scenarios [15–17]. Often, a higher-resolved North American regional atmospheric model such as the NACORDEX (North American component of the international CORDEX (Coordinated Regional Downscaling Experiment)) [18], or WRF (Weather Research and Forecasting model) [19] is used in these studies and compared with a courser resolution global model [20]. Recently, there have been observations that winds, including surface winds, are slowing globally. A recent review paper suggests that the data supporting this claim might be region-specific, and more information about internal modes of climate and changes to land use and land cover is needed before understanding this theoretical trend

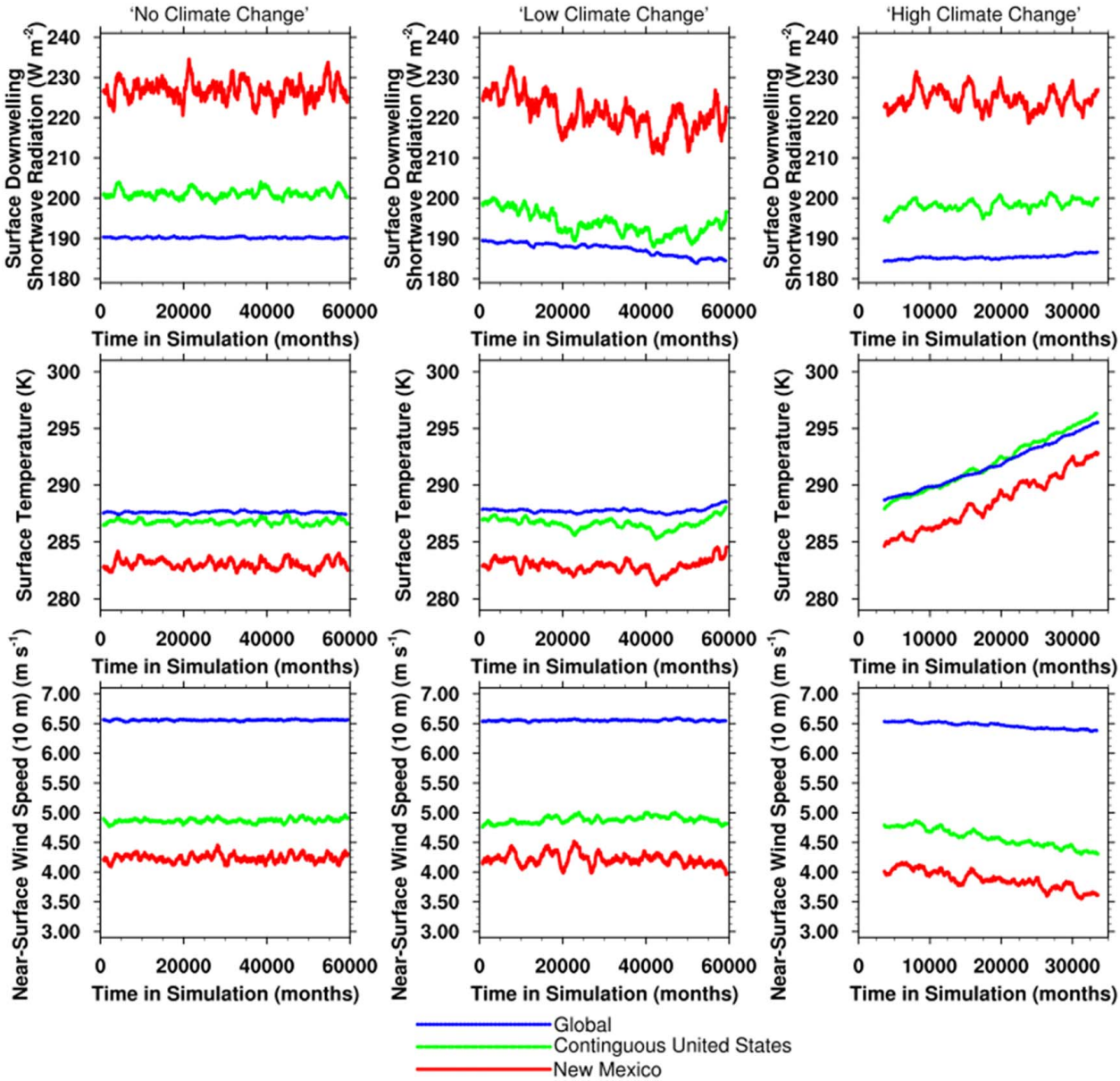

Fig. 2 Time series of the surface downwelling shortwave radiation, surface temperature, and near-surface wind speed for the "No Climate Change" (ECA_piControl), "Low Climate Change" (historical), "High Climate Change" (SSP585) CMIP6 E3SM simulations for global, contiguous United States, and New Mexico areas. The time series represents monthly means from the simulation data, and the data were smoothed by applying a 48-point running average

[21]. The previous works considered for comparison here did not mention the observational trend of wind stillness in their findings.

For solar power, there appears to be no agreement that solar resources will increase or decrease for a given future, warmer climate across the western United States [17,22–25]. Even comparisons using 37 earth system models run under the CMIP5 protocols showed an increase in solar production for the southern United States. However, when 14 regional climate models (i.e., higher spatial resolution) were used, the solar production was calculated to decrease [26]. Although unresolved cloud behavior seems to be a likely culprit in explaining the differences between the global and regional models, differences in cloud properties alone could not explain differences, so it was assumed aerosols were also playing a role with an approximately $\pm 2.5\%$ change in solar radiation at the surface. However, it should be noted that aerosol concentrations and pathways contain high uncertainty and speculation in future climate projections.

For general climate model bias as it relates to observations, climate modeling groups publish simulated model bias compared to global observations. The climate model used in this work, E3SM, has reported a negative bias of shortwave (visible) cloud radiative effects compared to observations, but with little-to-no precipitation bias compared to global satellite observations. This could imply that E3SM rains out the simulated cloud, leaving too-little cloud mass after a precipitation event. Additionally, E3SM has a strong aerosol-related effective radiative forcing and a high equilibrium climate sensitivity. This means the SSP585 scenario is likely to project a warmer earth than other models at the end of the simulation in the year 2100.

2.4 Climate Modeling Discussion. In gathering information needed to compute future climate change scenarios, a list was developed of potential future work that could analyze details of future climate change impacts on renewable energy production.

Table 3 Averages and standard deviations of solar radiation, surface temperature, and surface wind from E3SM CMIP6 scenarios

Variable	Scenario	Average	Standard deviation
Solar, rsds (W m^{-2})	No climate change	226.7	75.21
	Low climate change	221.0	76.51
	High climate change	224.4	75.56
Surface temperature, *Ts* (K)	No climate change	283.0	9.250
	Low climate change	283.1	9.244
	High climate change	288.5	9.613
Surface wind, sfcWind (m s^{-1})	No climate change	4.239	0.7831
	Low climate change	4.215	0.8471
	High climate change	3.871	0.8012

Table 4 Wind resources in New Mexico

Existing wind power purchase agreement resources	County	Net capacity (MW)	Turbine capacity (MW)	Hub height (m)
NM Wind Energy Center	Quay	200	1.5	80
Casa Mesa Wind	Quay	50	2.5	89
La Joya 1	Torrance	166	2.5	89
La Joya 2	Torrance	140	2.5	89
Red Mesa Wind	Sandoval	102	1.6	80

- Models that have high spatial and temporal resolution produce different trends than global models. Despite high variability and uncertainty, understanding the benefits of additional information at the cost of computer time is still undetermined for New Mexico [16]. Understanding downscaling for this problem is needed.
- In the CMIP6 database, the climate variable standards for solar radiation did not separate the GHI, into terms of DHI and DNI, $GHI = DHI + DNI \cdot \cos(z)$. Understanding predictions and baseline results of diffuse and direct will help understand model bias in changes in aerosol optical depth and cloud cover.
- The results presented here are monthly means which do not account for nighttime and daytime differences with high time-resolved data sets. For solar power production, nighttime values will be different than daytime, and wind production might also change over a diurnal cycle. Finding data in the CMIP6 archive or going to individual model output will clarify the computed answers and could change the uncertainty distribution.
- Wind turbines have cut-in and cut-out speeds. Higher time-resolved values for wind will show when wind speed is too great for turbines.
- Although this is not expected to change the findings of this report, using data from the CMIP6 archive that has more vertical levels, or altitude values, so that hub height and not sfcWind is used to calculate the wind power generation.
- Trends for wind slowing and stillness over New Mexico should be investigated in both observational data and simulated future climate projections.
- The E3SM baseline simulation (i.e., the preindustrial control) should be compared to reanalysis and other weather-based data sets to improve the understanding of the baseline bias.
- Other studies have used field-acquired data with machine learning sorting algorithms to determine potential weather impacts on renewable energy production [27]. Given the difficulty of earth system models to simulate extremes, linking realistic data with future projections is an area of potential research.

Table 5 List of PRC-approved and pending-approval large solar arrays in New Mexico

Site	AC Capacity (MW)	Status
Arroyo	300	PRC-approved
Jicarilla 1	50	PRC-approved
San Juan	200	PRC-approved
Rockmont	100	PRC-approved
Atrisco	300	Submitted Application
Jicarilla 2	50	Submitted Application
Sky Ranch	190	Submitted Application
Encino North	50	Submitted Application

- How can the unresolved clouds, and uncertainty in cloud cover be accounted for? Jiménez et al. [28] looked at 6 h ensemble simulations with WRF Solar for unresolved cumulus with observations and found that parameterizing radiative effects of deep and shallow cumulus is necessary to reduce a 55% overprediction in GHI. A positive GHI bias has been reported in WRF over Albuquerque, New Mexico [19]. How can this cloud bias be accounted for in global earth system models?

Other options for increasing resolution include using variable or refined resolution atmospheric models. These configurations could also be linked with Sun4Cast and weather prediction to compute solar variability [24]. Wang et al. [29] used CESM-VR with clustering for wind resources over California and found statistically significant changes in capacity. They found through clustering weather patterns that over a 36-year period, wind regimes occurring on "hot summer days increased at half a day per year and stagnant conditions increased at one-third days per year." Using downscaled MERRA with WRF and energy firm data helped drive this finding [30].

3 Climate Change Impacts on Solar and Wind Power Generation

3.1 Wind and Solar Resources in New Mexico. Table 4 summarizes the existing wind resources in NM operated by PNM, and Table 5 summarizes the existing and pending solar resources in NM operated by PNM. The older wind turbines are at a hub height of 80 meters, and the newer ones are at 90 meters. PNM will likely add more wind in the future, but the timing and amount are uncertain. Additional wind capacity will probably also be in Torrance County (near Clines Corners) because of access to PNM transmission.

3.2 Impact of Modeled Climate Change on Public Service Company of New Mexico Wind Power Generation. Using hourly 2012 wind speed data [31] for a point representing the NM Wind Energy Center wind generator (204 MW installed capacity), we found that that a drop of 8.7% in wind speed each hour yielded a *13% drop in total wind energy output* for the year. The following sections describe these findings.

3.2.1 Methodology. The 2012 wind speed data for a site representing the NM Wind Energy Center were obtained on an hourly basis from the Wind Prospector [31]. Specifically, wind speed data for the cell located at lat: 34.65, long −104.04 (Site ID: 874603 on the Wind Prospector [31]) was downloaded on an hourly basis for 2012. Turbines are classified as Class I, II, or III with average design wind speeds of 10, 8.5, and 7.5 m/s, respectively, as outlined in the International Electrotechnical Commission (IEC) 61400-1 standard [32].

The wind power equation can be expressed as follows: Power (W) = ½ ρ A V^3 C, where ρ = air density (~1.2 kg/m^3 at sea level), V = velocity in (m), A = area swept by the wind turbine

blades (m^2), and C = ratio of power extracted by wind turbine to total available in the wind resource, where 0.59 (the Betz Limit) is the theoretical maximum [33]. Because the kinetic power available in wind is proportional to the cube of the wind velocity, a wind turbine experiencing 9 m/s winds is exposed to more than three times the force of a wind turbine experiencing 6 m/s winds. It would not be economical to design turbines for low-wind sites to the same standards as high-wind sites; therefore, different design standards were established for sites with different average levels of wind.

Because Class II turbines are the most common, this study determined how changes in wind speed impact the power production for Class II turbines using a wind-speed-to-power conversion curve [34] (Fig. 3). Wind speed data were not obtained for each individual wind turbine—the simplifying assumption was that since we are interested in the difference between generation at a reference wind speed and a post-climate change wind speed, it is reasonable to not take individual turbine locational differences into account.

The wind-farm output in each hour was calculated using the Wind Prospector dataset for wind speed in 2012 as input to the power curve in Fig. 3. The wind velocity in that data set was reduced in each hour by 8.7% to reflect the modeled change in the High Climate Change scenario. Comparing the total amount of power generated in the reference case to the High Climate Change scenario, the study team found that the 8.7% drop in wind speed in each hour led to *an overall 13% drop in wind generation output*.

The annual capacity factor calculated for the wind farm (using a single-point representation of that wind farm) was calculated at 50% for the reference case and 43.5% for the High Climate Change scenario; 50% is an unusually high capacity factor for a wind farm and suggests that more detailed modeling may be warranted. Nevertheless, we are more interested in the difference between the two scenarios. It is reasonable that the percentage decline in power generation should be greater than the percentage decline in wind speed.

An 8.7% reduction in wind speed in each hour does not yield an 8.7% reduction in power output because the wind speed to MW output conversion formula is not linear. Also, there is about a 30% decrease in the number of hours the wind speed is 11 m/s or more (which is the point above which power output is at full capacity). There is also an increase in the number of hours the wind speed is 4 m/s or less (the point where wind power output is zero). The net effect is that there are about 11% more hours where the wind speed does not yield a 100% or a 0% capacity factor but is along the variable portion of the curve. In addition, the slope in the middle of the curve is quite steep—going from 7 m/s to 8 m/s causes output to increase by about 50% (from 31 MW to 47 MW for a 100 MW wind farm).

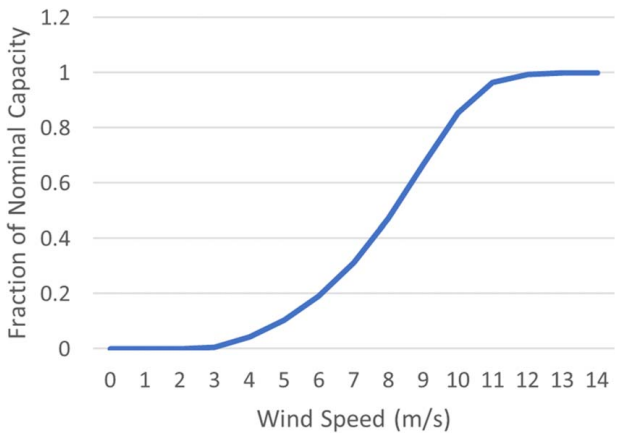

Fig. 3 Power curve for IEC Class II Turbine

3.3 Impact of Modeled Climate Change on Public Service Company of New Mexico Solar Power Generation. The potential impact of climate change on PNM solar power generation was modeled using two different methods. One method (called the "Specific" method) involved calculating the output for the Arroyo solar plant given 5 min satellite weather data and then adjusting the solar irradiance and increasing the ambient temperature by the climate-change-scenario amounts. Another method (called the "General" method) focused on calculating the impact of climate change on a generic solar PV facility.

The two methods arrived at the same conclusion—a 2.5% drop in solar irradiance and a 5.5 °C rise in ambient temperature (in all hours) would result in roughly a *4% drop in solar PV generation.* Based on results from the Specific method, about half of this drop is due to the decrease in solar irradiance, and about half is due to PV efficiency loss from higher ambient temperatures. The following sections provide more details.

3.3.1 Climate Scenario Selection. Based on the climate modeling results given in Table 3, we see that a simulated worst-case scenario for solar PV power production would be a 2.5% drop in solar irradiance (with solar irradiance dropping from 226.7 W/m^2 in the reference case to 221.0 W/m^2 in the "Low Climate Change" case), and a 5.5 °C increase in average ambient temperature (10 °C average in the reference case to 15.5 °C in the "High Climate Change" case). A great deal of uncertainty exists in these preliminary climate models, and it is possible that actual climate change impacts may be less or greater than our simulated "worst-case." Our primary goal was to develop a methodology and framework that can be used for future analyses with more refined climate models and data.

3.3.2 Methodology—Specific Method. A single, large solar PV plant was modeled using pvlib python, which is a community-supported tool that allows for detailed simulation of the performance of photovoltaic energy systems [35]. It was originally taken from the PVLIB MATLAB toolbox developed at Sandia National Laboratories and implements many of the models and methods developed there.

The location chosen for the plant was the site of the future Arroyo solar PV power plant (in McKinley County, NM—about 10 miles East of the Chaco Culture National Historical Park). Given that this plant is the largest plant approved by the NM PRC to date, and that it is a single-axis tracking plant (as all future PV plants for PNM are likely to be), we felt that this plant is sufficiently representative of the PV plants that will make up most of PNM's solar PV plant capacity in the future and that it can be used as a proxy for PNM solar PV plants in general.

Solar irradiance (and ambient temperature) data were downloaded from the National Solar Radiation Database (NSRDB) [36] at a five-minute resolution for the cell with coordinates 35.96 deg latitude and −107.63 deg longitude. This cell represents an area of 4 km^2 (as the spatial resolution is 2 km by 2 km). The NSRDB identifier for this cell is 787,961.

The solar irradiation data used in this model, specifically, are DHI, DNI, and GHI, all expressed in W/m^2. DHI is the amount of radiation received per square meter by a surface (not subject to any shade) that does not arrive on a direct path from the sun (in other words, light that is scattered by molecules in the atmosphere). DNI is the solar radiation per square meter by a surface that is always perpendicular to the light coming straight from the sun (given its current position in the sky). GHI is the total amount of shortwave radiation received from above by a surface horizontal to the ground. The relationship between these three measurements of solar irradiation is given by $GHI = DNI \times \cos(\theta) + DHI$, where θ is the solar zenith angle (directly overhead would be $\theta = 0$).

The PV system simulated in pvlib python was assumed to be a single-axis tracking plant with an inverter load ratio (ILR) of 1.3. In other words, the PV panel capacity for this plant was set at 1.3 times the capacity of the AC inverter. The actual Arroyo plant will, in fact, have an ILR of 1.3, and it is likely that future solar

PV plants providing power will have a similar ILR. This is because it is not economical to size the inverter at the full output capacity of the PV panels, as this full capacity would be used only for a small fraction of time. In addition, setting the inverter at a smaller size than the PV panels allows for a more even power output profile in the middle of the day.

The system size chosen was a normalized 1.34 MW DC, 14 MW AC system. First, the reference case was generated by loading in the five-minute solar irradiance and ambient temperature data for 2018 and running the model. The model generated an AC power output data set for a year (at a five-minute resolution) based on the plant type, location, solar irradiance, and ambient temperature data given.

Next, the climate change cases were generated by modifying the weather inputs to account for a Low Climate Change scenario, a High Climate Change scenario, and a Combination scenario. Specifically, GHI, DHI, and DNI were reduced at all times by the amount specified in each scenario, and the temperature was increased at all times by the average ambient change specified. New model runs were made which took this modified weather data as input and produced new AC power output data sets for a year (also at a five-minute resolution). The power output for each scenario run was summed over the year, and the total annual power generated was compared with the reference run. The changes used for these scenarios, as well as the results of the model runs, are summarized in Table 6.

The Combination scenario, which posits a 2.5% drop in solar irradiation and a 5.5 °C rise in ambient temperature, led to roughly a 4% decrease in solar PV power production as compared to the reference run.

3.3.3 Methodology—General Method. In this method, the cell temperature (Tcell) is calculated based on the insolation (S), the ambient temperature (Tamb), and the normal operating cell temperature (NOCT) that is measured at 800 W/m^2 and 20 °C ambient as follows:

$$T_{cell}\ (^{\circ}C) = T_{amb} + (\mathrm{NOCT} - 20) \times S/800 \tag{1}$$

Therefore, given ambient temperature and insolation differences, the cell temperature change can be calculated as following:

$$\Delta T_{cell} = \Delta T_{amb} + (\mathrm{NOCT} - 20) \times \Delta S/800^{\circ}\mathrm{C} \tag{2}$$

Since power-temperature coefficient, C (% per °C) of a PV panel is often given based on testing data, and the percentage change in output generation of the PV panels can be specified

$$\Delta P_{out}\ (\%) = C \times \Delta T_{cell} \tag{3}$$

Given 5.5 °C ambient temperature rise, around 2.5% insolation reduction and −0.3% power-temperature coefficient, the overall reduction in annual generation of PV system is calculated and compared with the baseline case. The results show that PV generation drops about 4%, same as the Specific Method.

4 Climate Change Impacts on Battery Storage

Operating temperature is one of the main factors that significantly affect the life span as well as the performance of li-ion batteries (LiB). While high temperature increases the formation and modification of the surface film on batteries' electrodes making them degrade faster, low temperature slows down the electrochemical reactions within the batteries making them less efficient. Furthermore, extremely low or high temperature can also create serious damage to LiBs. Therefore, for grid-scale battery energy storage systems (BESS), heating, venting, and air conditioning (HVAC) systems are often required to maintain the battery enclosure's temperature within an operating range. Since the change in ambient temperature will impact HVAC's operation, it will also impact the overall performance of a BESS.

Table 6 Solar PV scenarios and results

Scenario	Change in solar irradiation	Change in average ambient temperature	Annual drop in solar output
Low climate change	−2.5%	0 °C	1.9%
High climate change	−1%	+5.5 °C	2.9%
Combination	−2.5%	+5.5 °C	4.1%

4.1 Impact of Temperature Change on Battery Storage. In this section, the impact of climate change is seen as the impact of ambient temperature rise on the performance and degradation of Li-ion BESS. Three scenarios of temperature rise are considered including the following:

- Scenario 1—Nominal: this scenario assumes the ambient temperature would not change in the next 24 years. This is used as the baseline to evaluate the other two scenarios.
- Scenario 2—Moderate temperature rise: this scenario considers 2 deg temperature rise in the next 24 years.
- Scenario 3—Extreme temperature rise: this scenario considers 5 deg temperature rise in the next 24 years.

Grid-scale Li-ion BESSs are required to sit outdoors by the current safety codes. Therefore, these BESSs are often packed as modules that are contained in standard shipping containers. The module size often varies with applications and manufacturers; however, in this work, we model a typical 1 MW/4 MWh module contained within a 20 ft standardized shipping container. Just as modules can be stacked to achieve a larger system, so too this model can be scaled to model the systems of different sizes. The purpose of this model is to study the overall performance of BESS given the ambient temperature and the loading (charge/discharge) profile of the BESS. For simplification, the following assumptions are made:

- BESS alternatively charges and discharges every 12 h;
- BESS loss is purely heat loss;
- Battery temperature is equal to the enclosure temperature;
- The container is not insulated.

The input parameters of the model are given in Table 7.

The container's change in temperature, ΔT (K), at each time-step, i, is calculated using an energy balance

$$\Delta T_i = \frac{\dot{E}_{in,i} - \dot{E}_{out,i}}{mc_p}\Delta t \tag{4}$$

where $\dot{E}_{in,i}$ is the heat generation (W) caused by the battery inefficiency (assumed to be lost entirely to resistive heating) during

Table 7 Parameters used in HVAC modeling of BESS power consumption

Parameters	Unit	Value
BESS Power rating	MW	1
BESS Energy capacity	MWh	4
LiB Specific weight	Wh/kg	160
Mass, m	kg	25,000
Round-trip efficiency	%	90
One-way efficiency	%	95
BESS Specific heat, c_p	J/kg.K	1000
HVAC Capacity	BTU/h	80,000 (23,400 W)
Container surface area	m^2	67.63
Container emissivity	–	0.8
HVAC Power rating	W	8000
HVAC Duty cycle	%	40
HVAC Max coefficient of performance	–	4

charging and discharging, $\dot{E}_{out,i}$ is the heat dissipation from radiation and conduction from the shipping container and convection via HVAC, m is the mass of the BESS and container (kg), c_p is the specific heat (J/kg-K), and $\Delta t = 1$ h (3600 s). In the model, the HVAC is on at its rated power if the container's temperature is above 45 °C, off if the temperature is below 25 °C, and holding its status (on or off) if the temperature is decreasing below 45 °C or increasing above 25 °C. In each scenario, the model is used to simulate the container temperature at each hour throughout a year. The HVAC's energy consumption for a 4 MWh BESS is calculated accordingly and compared between different scenarios. The results are shown in Table 8.

As seen in Table 8, the HVAC annual energy consumption increases as the temperature rises. This is because ambient temperature rise will reduce the heat dissipation through radiation, convection, and conduction making the HVAC work harder to maintain the operating temperature range. Significant increase in HVAC energy consumption will increase the overall load of the system thereby decreasing the net impact of BESSs. However, the relative impact of an ambient temperature rise of up to ∼5 °C on increased HVAC energy consumption is predicted to yield less than 1% change in the total annual battery throughput energy. Therefore, the uncertainty on increased temperatures on HVAC parasitic power consumption is not directly included in the probabilistic simulations; the uncertainty is assumed to be subsumed by the uncertainty in the capacity fade and round-trip efficiency described in the following section.

4.2 Impacts of Capacity Fade and Round-Trip Efficiency on Battery Storage. Capacity fade and round-trip efficiency can impact the available throughput energy of battery storage systems. Although not necessarily tied to climate change, this study included uncertainty in capacity fade and round-trip efficiency in the probabilistic simulations.

Capacity fade is a condition in which the total energy capacity that a battery can deliver reduces with use and is dependent on a number of factors including ambient temperature, discharge rate, and depth of discharge. Preger et al. [37] performed a multi-year test of different lithium-ion cells under varying discharge conditions and found that the number of cycles to reach an 80% capacity (20% capacity loss) ranged from only a few hundred cycles to several thousand cycles, depending on cell type and conditions. Spotnitz [38] reported that among different lithium-ion cell types, the capacity loss at 500 cycles ranged from ∼12 to 24%. Based on these studies, we assume that the capacity loss of battery storage systems used by PNM may be up to 20% within a few years of deployment—before issues are identified and servicing or replacement of cells can be performed. A uniform distribution for battery capacity fade between 0 and 20% was therefore assumed and sampled for each annual realization of the hourly energy balance.

Table 8 Modeled annual HVAC energy consumption as a function of ambient temperature rise

Climate Scenario (ambient temperature)	HVAC Annual energy consumption (MWh)	HVAC Annual energy consumption change (%)	Ratio (%) of HVAC annual energy consumption to annual battery throughput energy[a]
Current conditions	23.5	0	1.6%
2 °C Increase	25.0	12.1%	1.7%
5 °C Increase	27.3	22.4%	1.9%

[a]Four MWh/discharge × 365 discharges/year = 1460 MWh of annual battery throughput energy.

This sampled value was used to reduce the total battery storage capacity prescribed in the 2040 No New Combustion scenario.

Preger et al. also evaluated the round-trip efficiency (energy out/energy in) of various lithium-ion cells and found that the initial round-trip efficiency varied between ∼80% and 95%. After cycling to a capacity loss of 20%, the decrease in initial round-trip efficiency ranged from less than a few percent up to ∼10% in many reported cases. Based on these studies, the round-trip efficiency (and impacts of potential degradation) for the battery systems used by PNM during any year in the probabilistic simulations was assumed to be uniformly distributed between 80% and 95%. The sampled round-trip efficiency was used to reduce amounts of energy added to the battery during any hour when supply exceeded demand for the No New Combustion scenario. For example, if the sampled round-trip efficiency for a given year was 90%, and the energy supply exceeded demand by 10 MWh during a given hour, the energy stored during that hour for later delivery was set equal to 0.9×10 MWh $= 9$ MWh (assuming that the total energy stored did not exceed the total nameplate capacity of all available battery storage systems, accounting for capacity fade described earlier).

5 Probabilistic Analysis of Climate Change Impacts and Battery Performance

5.1 Modeling Approach. At each hour of the year starting at 12 a.m. January 1 and ending at midnight December 31, the energy, E_i (MWh), produced from all available generation sources in the 2040 No New Combustion scenario were summed, including uncertainty in intermittent wind and solar resources as impacted by climate change modeling. In addition to variable solar and wind generation at each hour of the year, firm fixed resources (i.e., nuclear, geothermal) were added as prescribed by PNM (see Table 9). If the total generation exceeded the total load, L_i (MWh), at any hour, surplus generation was added to the battery storage (after adjustment for round-trip efficiency). If the generation was less than the load at that hour, energy was taken from battery storage. Checks were implemented to determine the minimum and maximum state of charge (SOC) of the battery storage system (in MWh) at each hour: (1) if generation was less than the load, and total SOC decreased to a value less than zero, the SOC was set to zero, and (2) if generation was greater than the load, and SOC increased to a value greater than the maximum battery storage capacity adjusted for capacity fade (*Fade*), the SOC was set equal to the maximum battery storage adjusted for capacity fade and battery round-trip efficiency (*RTE*). The SOC at the start of the year was assumed to be equal to 100%. The steps to calculate the SOC at each hour can therefore be summarized as follows:

$$\mathrm{SOC}_i = \mathrm{SOC}_{i-1} + \sum_i E_i - L_i \tag{5}$$

Table 9 Summary of firm fixed resources assumed for PNM 2040 No New Combustion scenario (in addition to solar and wind generation) [9]

Parameter	Value
Total energy efficiency[a] (MW):	95
Total demand response[b] (MW):	15
Total coal resources (MW):	0
Total nuclear resources (MW):	288
Total natural gas resources (MW):	0
Total geothermal resources (MW):	11
Total battery storage resource (MWh):	14,328
% battery capacity on Jan. 1 (hour 1):	100%

[a,b]Not used in probabilistic hourly energy balance.

$$\text{If } SOC_i < 0, \quad SOC_i = 0$$

$$\text{else if } SOC_i > SOC_{max}(1 - Fade_j), \quad SOC_i = SOC_{max}(1 - Fade_j)RTE_j$$

$$\text{else if } \sum_i E_i - L_i > 0, \quad SOC_i = SOC_{i-1} + \left(\sum_i E_i - L_i\right)RTE_j$$

where i is the hour of the year (1–8760) and j is the realization (1–100).

Uncertainty distributions of wind and solar generation, battery RTE, and battery fade (Table 10) were sampled to create 100 realizations of annual energy balances for the 2040 No New Combustion scenario. All other input parameters (e.g., firm fixed resources, load) were not varied from the baseline values.

In each realization, the LOLE was determined as the number of days (hours divided by 24) in which the SOC was equal to zero during the year. The cumulative distribution function for the LOLE was plotted for all 100 realizations. The goal was to determine if the distribution of LOLE was significantly greater than the desired value of 0.2 days/year or less with the impacts of climate change and uncertainty in battery performance. If so, a sensitivity study would be performed to determine the additional battery storage capacity required to reduce the LOLE to 0.2 days/year or less.

5.1.1 Uncertainty in Wind Energy Resources. Historical average wind generation capacity factors for each hour of the month were reported by PNM (2013–2019) [9], which reveals that wind generation typically peaks in the late afternoon and evening hours and subsides in the morning hours. Februrary through April are the most productive months for wind generation, while July and August are the least productive.

These hourly capacity factors were multiplied by the total expected wind generation capacity (9564 MW) in the 2040 most cost-effective No New Combustion portfolio presented in the PNM 2020–2040 IRP [9] to yield baseline wind power generation values at each hour of the year. For simplicity, the wind generation for a specific hour of any given month was assumed to be the same (e.g., the wind generation at 7 a.m. for each day in January was assumed to be the same; the wind generation at 3 p.m. for each day in July was assumed to be the same).

Uncertainty in these baseline values was accommodated by uniformly varying the baseline values by up to ±50% in the probabilistic simulations as summarized in Table 10. Although arbitrary, this uncertainty range was thought to be appropriate to accommodate uncertainty in not only the natural variability in wind generation but also the unceratinty in the preliminary climate models. A sensitivity was also performed to determine the impacts of varying the uncertainty range on LOLE.

5.1.2 Uncertainty in Solar Energy Resources. Historical average solar-generation capacity factors for each hour of the month were reported by PNM (2013–2019) [9]/Solar generation peaks around the 12th hour of the day (standard time) and is highest during the spring/summer months and lowest during the winter months. These hourly capacity factors were multiplied by the total expected solar-generation capacity in the 2040 most cost-effective No New Combustion portfolio presented in the PNM 2020–2040 IRP [9] to yield baseline solar power generation values at each hour of the year. For simplicity, the solar generation for a specific hour of any given month was assumed to be the same (e.g., the solar generation at 3 p.m. for each day in July was assumed to be the same). Uncertainty in these baseline values was accommodated by uniformly varying the baseline values by up to ±50% in the probabilistic simulations as summarized in Table 10. Although arbitrary, this uncertainty range was thought to be appropriate to accommodate uncertainty in not only the natural variability in solar generation but also the unceratinty in the preliminary climate models. A sensitivity was also performed to determine the impacts of varying the uncertainty range on LOLE.

Table 10 Summary of uncertainty distributions in probabilistic simulations

Parameter	Nominal value[a]	Uniform distribution	
		Minimum	Maximum
Wind generation (MWh)	−13%	−50%	+50%
Solar generation (MWh)	−4%	−50%	+50%
Battery RTE	N/A	80%	95%
Battery capacity fade	N/A	0%	10%

[a]The nominal value for wind and solar generation represents the impact of climate change (see Secs. 3.2 and 3.3) on baseline values provided by PNM using their historical capacity factors and expected generation capacity in the 2040 No New Combustion portfolio (see Secs. 0 and 5.1.2).

5.1.3 Uncertainty in Battery Storage Resources. Table 11 shows the planned battery storage systems in PNM's No New Combustion portfolio. The total energy capacity (MWh) of each system was calculated as the product of the power capacity (MW) and storage duration of each system. The total energy storage capacity was used in the hourly energy balance calculations. Uncertainty in the battery storage capacity and performance was included by sampling the capacity fade and RTE for each annual realization using the uncertainty distributions in Table 10 and applying those to the conditions in Eq. (5).

5.1.4 Annual Energy Load. PNM provided the reference forecast for hourly electricity loads to Sandia. For each month, the loads at a particular hour of each day were averaged. Therefore, the hourly load for a particular time each day during a given month were assumed to be the same. For example, the load at 10 a.m. for each day in March was assumed to be the same. The loads in 2040 were approximately 6% higher than the reference loads in 2020.

5.2 Modeling Results. Results showed that the baseline LOLE (assuming 100% battery performance including 100% RTE and no capacity fade) was 0 days/year with the assumed generation resources, loads, and an assumed initial battery SOC (hour 1 of the year) of 100%.[2] The probabilistic simulations using uncertainty distributions summarized in Table 10 yielded a median LOLE of ∼2 days/year and a 95th percentile of LOLE of ∼8 days/year. A sensitivity study that reduced the uncertainty distribution for the wind and solar generation from +/−50% to +/−25% about the nominal climate-impacted value yielded a similar median LOLE of ∼2 days/year and a 95th percentile of LOLE of

Table 11 Summary of planned battery storage systems in PNM's No New Combustion, most cost-effective portfolio [9]

Storage system[a]	Nameplate capacity (MW)		
	2021	2030	2040
Arroyo Storage ESA (MW)	0	150	150
Jicarilla Storage ESA (MW)	0	20	20
Rockmon Storage ESA (MW)	0	30	30
San Juan Storage ESA (MW)	0	100	100
New Lithium-Ion Battery (4 h) (MW)	0	508	1025
New lithium-ion battery (8 h) (MW)	0	262	391
New flow battery (10 h) (MW)	0	0	590
New pumped storage (MW)	0	0	0
Total storage capacity (MWh)	0	5328	14,328

[a]ESA (Energy Storage Agreement) storage systems were assumed to be 4-h Li-ion batteries for calculating energy capacity.

[2]An initial SOC of 0% increased the LOLE to 0.33 days/year for the baseline case. An initial SOC of 10% resulted in an LOLE of 0.2 days/year.

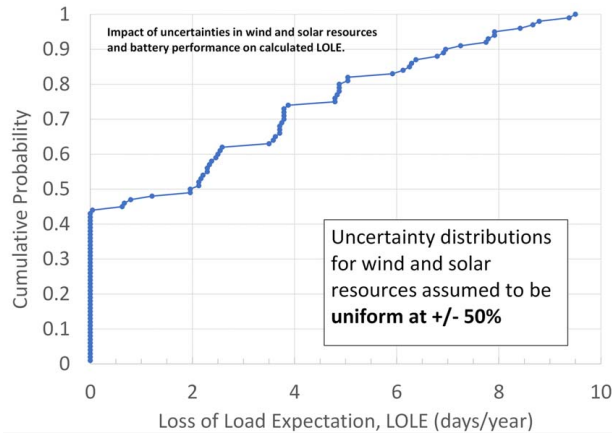

Fig. 4 Cumulative probability of loss of load expectation (LOLE) with inclusion of solar and wind resource uncertainty resulting from climate change and uncertainty in battery performance. *Uniform* distributions of ±50% were assumed for the solar, wind, and battery performance uncertainty distributions.

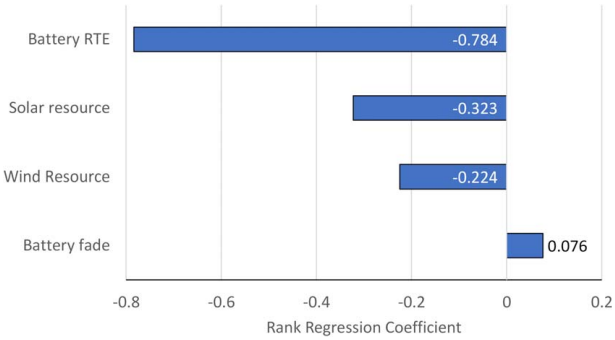

Fig. 5 Impact of uncertainties in solar and wind resources and battery performance resulting from climate change on LOLE. Standardized rank-regression coefficients are shown.

~7 days/year. Figure 4 shows the cumulative distribution functions of LOLE for the probabilistic simulations.

Figure 5 shows the results of a rank-regression analysis to determine the impact of uncertainties in the wind and solar resources and battery performance (RTE and capacity fade) on the LOLE using the +/−50% uniform uncertainty distribution for wind and solar resources. Results show that the battery RTE was the most significant parameter that impacted LOLE, followed by solar resource, wind resource, and battery fade. Figure 6 shows the incremental coefficients of determination for the uncertainty parameters. Uncertainty in the battery RTE yielded the greatest variability in the LOLE, followed by solar resource, wind resource, and battery fade. Similar results were obtained when a +/−25% uncertainty distribution was assumed.

A sensitivity study was performed to determine how much battery storage capacity was required to reduce the LOLE to 0.2 days/year. In order to reduce the median (50th percentile) LOLE to 0.2 day/year, the battery storage capacity had to be increased from the baseline value of 14,328 MWh to ~25,000–30,000 MWh, about a factor of two higher than the baseline value assumed by PNM. In order to reduce the 95th percentile of LOLE to 0.2 day/year, the battery storage capacity had to be increased to ~100,000 MWh, about a factor of seven times higher than the baseline value.

6 Conclusion and Recommendations

New Mexico's Energy Transition Act (ETA) requires power utilities in New Mexico to increase their share of carbon-free

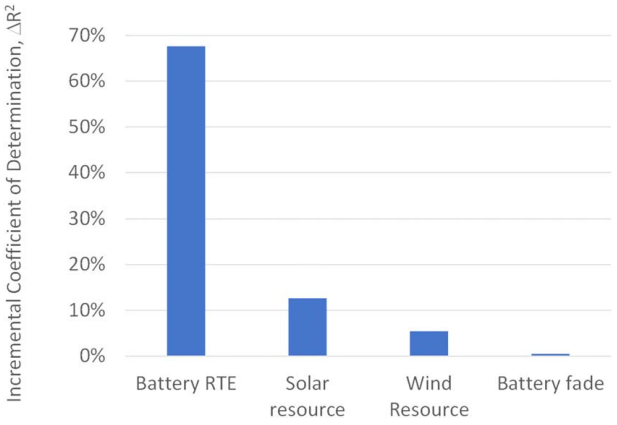

Fig. 6 Impact of uncertainties in solar and wind resources and battery performance resulting from climate change on LOLE variability. Incremental coefficients of determination are shown.

electricity generation to 50% by 2030, 80% by 2040, and 100% by 2045. According to its 2020 Integrated Resource Plan, PNM's plan is to rely heavily on utility-scale PV and wind generation with battery energy storage to meet these requirements in the most cost-effective portfolio with no new combustion. The objective of this work was to develop a methodology to evaluate the potential impacts of climate change on wind and solar resources, as well as uncertainties in battery performance, on the annual LOLE.

Key points and results from this study were as follows:

- For the extreme climate change scenario, the projected wind power may decrease by ~13% due to projected decreases in wind speed. Projected solar power may decrease by ~4% due to decreases in irradiance and increases in temperature in NM.
- Uncertainty in these climate-induced changes in wind and solar resources was accommodated in probabilistic models assuming uniform distributions in the annual reductions in solar and wind resources. Uncertainty in battery storage performance was also evaluated based on increased temperature, capacity fade, and degradation in round-trip efficiency.
- The hourly energy balance was determined throughout the year given uncertainties in the renewable energy resources and energy storage.
- The LOLE was evaluated for the 2040 No New Combustion portfolio and found to increase from 0 days/year to a median value of ~2 days/year due to potential reductions in renewable energy resources and battery storage performance and capacity.
- An increase in battery storage capacity to ~30,000 MWh from a baseline value of ~14,000 MWh was required to reduce the median value of LOLE to ~0.2 days/year with consideration of battery degradation and potential climate impacts on solar and wind resources.
- A rank-regression analyses revealed that battery round-trip efficiency was the most significant parameter that impacted LOLE, followed by solar resource, wind resource, and battery fade.

The current work assumed projected electrical loads in 2040. Future work should investigate the potential impact of climate change on uncertainty in electrical loads. In addition, the current study evaluated the impact of increasing storage capacity on LOLE. Increased solar and wind capacity impacts on LOLE should be considered in future studies.

Acknowledgment

The authors thank Nick Phillips from PNM for providing data and consultation regarding this work. This work was funded by

the Climate Change Security Center program (278/40.02.01.04.02.01.06) at Sandia National Laboratories (Center 8900).

Conflict of Interest

There are no conflicts of interest.

Data Availability Statement

The data sets generated and supporting the findings of this article are obtainable from the corresponding author upon reasonable request.

Nomenclature

m = mass of the BESS and container (kg)
A = area swept by the wind turbine blades (m^2)
C = ratio of extracted power by wind turbine to total available wind resource
P = power (MW)
V = wind velocity in (m/s)
c_p = specific heat (J/kg-K)
E_i = energy generation at time-step i (MWh)
L_i = load consumption at time-step i (MWh)
T_{amb} = ambient temperature (°C)
T_{cell} = cell temperature (°C)
$\dot{E}_{in,i}$ = heat generation (W) caused by the battery inefficiency
$\dot{E}_{out,i}$ = heat dissipation from radiation and conduction from the shipping container and convection via HVAC
BESS = battery energy storage systems
CMIP6 = Climate Model Intercomparison Project—Version 6
CORDEX = Coordinated Regional Downscaling Experiment
DHI = diffuse horizontal irradiance
DOE = Department of Energy
DNI = direct normal irradiance
ETA = Energy Transition Act
E3SM = Exascale Earth System Model
ESA = Energy Storage Agreement
GHI = global horizontal irradiance
HVAC = heating, venting, and air conditioning
IRP = Integrated Resource Plan
ILR = Inverter Load Ratio
IPCC = Intergovernmental Panel on Climate Change
LiB = lithium-ion battery
LOLE = loss of load expectation
NSRDB = National Solar Radiation Database
NM = New Mexico
NOCT = normal operating cell temperature
piControl = preindustrial control
PNM = Public Service of New Mexico
PRC = Public Regulation Commission
PV = photovoltaic
RTE = round-trip efficiency
SOC = State of charge of storage system
SSP585 = highly warming simulation
WRF = weather research and forecasting
Δt = time-step (h)
θ = solar zenith angle
ρ = air density (~1.2 kg/m^3 at sea level)

[3]https://www.energy.gov/downloads/doe-public-access-plan. Sandia R&A No. 1691593.

References

[1] Solaun, K., and Cerdá, E., 2019, "Climate Change Impacts on Renewable Energy Generation. A Review of Quantitative Projections," Renewable Sustainable Energy Rev., **116**, p. 109415.
[2] Gernaat, D. E. H. J., de Boer, H. S., Daioglou, V., Yalew, S. G., Müller, C., and van Vuuren, D. P., 2021, "Climate Change Impacts on Renewable Energy Supply," Nat. Clim. Change, **11**(2), pp. 119–125.
[3] Russo, M. A., Carvalho, D., Martins, N., and Monteiro, A., 2022, "Forecasting the Inevitable: A Review on the Impacts of Climate Change on Renewable Energy Resources," Sustainable Energy Technol. Assess., **52**, p. 102283.
[4] Ayli, U. E., Özgirgin, E., and Tareq, M., 2021, "Solar Chimney Power Plant Performance for Different Seasons Under Varying Solar Irradiance and Temperature Distribution," ASME J. Energy Resour. Technol., **143**(6), p. 061303.
[5] Addo-Binney, B., Besada, W., and Agelin-Chaab, M., 2022, "Analysis of an Integrated Thermal Energy System for Applications in Cold Regions," ASME J. Energy Resour. Technol., **144**(1), p. 012104.
[6] Houchati, M., Beitelmal, A. H., and Khraisheh, M., 2022, "Predictive Modeling for Rooftop Solar Energy Throughput: A Machine Learning-Based Optimization for Building Energy Demand Scheduling," ASME J. Energy Resour. Technol., **144**(1), p. 011302.
[7] Yang, P., and Najafi, H., 2022, "A Comparative Study of Multi-Stage Approaches for Wind Farm Layout Optimization," ASME J. Energy Resour. Technol., **144**(10), p. 101302.
[8] Harang, I., Heymann, F., and Stoop, L. P., 2020, "Incorporating Climate Change Effects Into the European Power System Adequacy Assessment Using a Post-Processing Method," Sustainable Energy Grids Netw., **24**, p. 100403.
[9] Phillips, N., Reiman, M., Brunton, D., Gutierrez, S., and Heslop, J., 2021, *PNM 2020–2040 Integrated Resource Plan*, Public Service Company of New Mexico, Albuquerque, NM. https://www.pnmforwardtogether.com/irp, Accessed January 29, 2021.
[10] Burrows, S. M., Maltrud, M., Yang, X., Zhu, Q., Jeffery, N., Shi, X., Ricciuto, D., et al., 2020, "The DOE E3SM v1.1 Biogeochemistry Configuration: Description and Simulated Ecosystem-Climate Responses to Historical Changes in Forcing," J. Adv. Model. Earth Syst., **12**(9), p. e2019MS001766.
[11] Eyring, V., Bony, S., Meehl, G. A., Senior, C. A., Stevens, B., Stouffer, R. J., and Taylor, K. E., 2016, "Overview of the Coupled Model Intercomparison Project Phase 6 (CMIP6) Experimental Design and Organization," Geosci. Model Dev., **9**(5), pp. 1937–1958.
[12] Golaz, J.-C., Caldwell, P. M., Roekel, L. P. V., Petersen, M. R., Tang, Q., Wolfe, J. D., Abeshu, G., et al., 2019, "The DOE E3SM Coupled Model Version 1: Overview and Evaluation at Standard Resolution," J. Adv. Model. Earth Syst., **11**(7), pp. 2089–2129.
[13] Tebaldi, C., Debeire, K., Eyring, V., Fischer, E., Fyfe, J., Friedlingstein, P., Knutti, R., et al., 2021, "Climate Model Projections From the Scenario Model Intercomparison Project (ScenarioMIP) of CMIP6," Earth Syst. Dyn., **12**(1), pp. 253–293.
[14] Craig, M. T., Cohen, S., Macknick, J., Draxl, C., Guerra, O. J., Sengupta, M., Haupt, S. E., Hodge, B.-M., and Brancucci, C., 2018, "A Review of the Potential Impacts of Climate Change on Bulk Power System Planning and Operations in the United States," Renewable Sustainable Energy Rev., **98**, pp. 255–267.
[15] Craig, M. T., Carreño, I. L., Rossol, M., Hodge, B.-M., and Brancucci, C., 2019, "Effects on Power System Operations of Potential Changes in Wind and Solar Generation Potential Under Climate Change," Environ. Res. Lett., **14**(3), p. 034014.
[16] Losada Carreño, I., Craig, M. T., Rossol, M., Ashfaq, M., Batibeniz, F., Haupt, S. E., Draxl, C., Hodge, B.-M., and Brancucci, C., 2020, "Potential Impacts of Climate Change on Wind and Solar Electricity Generation in Texas," Clim. Change, **163**(2), pp. 745–766.
[17] Haupt, S. E., Copeland, J., Cheng, W. Y. Y., Zhang, Y., Ammann, C., and Sullivan, P., 2016, "A Method to Assess the Wind and Solar Resource and to

Quantify Interannual Variability Over the United States Under Current and Projected Future Climate," J. Appl. Meteorol. Climatol., **55**(2), pp. 345–363.
[18] Mearns, L., McGinnis, S., Korytina, D., Arritt, R., Biner, S., Bukovsky, M., Chang, H.-I., et al., 2017, "The NA-CORDEX Dataset, version 1.0," NCAR Climate Data Gateway, Boulder CO.
[19] Skamarock, W., Klemp, J., Dudhia, J., Gill, D., Barker, D., Wang, W., Huang, X.-Y., and Duda, M., 2008, A Description of the Advanced Research WRF Version 3, UCAR/NCAR, 1002 KB 2008-06.
[20] Chen, L., 2020, "Impacts of Climate Change on Wind Resources Over North America Based on NA-CORDEX," Renewable Energy, **153**, pp. 1428–1438.
[21] Pryor, S. C., Barthelmie, R. J., Bukovsky, M. S., Leung, L. R., and Sakaguchi, K., 2020, "Climate Change Impacts on Wind Power Generation," Nat. Rev. Earth Environ., **1**(12), pp. 627–643.
[22] Crook, J. A., Jones, L. A., Forster, P. M., and Crook, R., 2011, "Climate Change Impacts on Future Photovoltaic and Concentrated Solar Power Energy Output," Energy Environ. Sci., **4**(9), pp. 3101–3109.
[23] Folini, D., Dallafior, T. N., Hakuba, M. Z., and Wild, M., 2017, "Trends of Surface Solar Radiation in Unforced CMIP5 Simulations," J. Geophys. Res. Atmos., **122**(1), pp. 469–484.
[24] Haupt, S. E., Kosović, B., Jensen, T., Lazo, J. K., Lee, J. A., Jiménez, P. A., Cowie, J., et al., 2018, "Building the Sun4Cast System: Improvements in Solar Power Forecasting," Bull. Am. Meteorol. Soc., **99**(1), pp. 121–136.
[25] Huber, I., Bugliaro, L., Ponater, M., Garny, H., Emde, C., and Mayer, B., 2016, "Do Climate Models Project Changes in Solar Resources?," Sol. Energy, **129**, pp. 65–84.
[26] Chen, L., 2021, "Uncertainties in Solar Radiation Assessment in the United States Using Climate Models," Clim. Dyn., **56**(1), pp. 665–678.
[27] Jackson, N. D., and Gunda, T., 2021, "Evaluation of Extreme Weather Impacts on Utility-Scale Photovoltaic Plant Performance in the United States," Appl. Energy, **302**, p. 117508.
[28] Jiménez, P. A., Alessandrini, S., Haupt, S. E., Deng, A., Kosovic, B., Lee, J. A., and Monache, L. D., 2016, "The Role of Unresolved Clouds on Short-Range Global Horizontal Irradiance Predictability," Mon. Weather Rev., **144**(9), pp. 3099–3107.
[29] Wang, M., Ullrich, P., and Millstein, D., 2020, "Future Projections of Wind Patterns in California with the Variable-Resolution CESM: a Clustering Analysis Approach," Clim. Dyn., **54**(3), pp. 2511–2531.
[30] Millstein, D., Solomon-Culp, J., Wang, M., Ullrich, P., and Collier, C., 2019, "Wind Energy Variability and Links to Regional and Synoptic Scale Weather," Clim. Dyn., **52**(7), pp. 4891–4906.
[31] National Renewable Energy Laboratory, "Wind Prospector," 2012 2021, https://maps.nrel.gov/wind-prospector.
[32] International Electrotechnical Commission, 2005, "Wind Turbines – Part 1: Design Requirements," International Standard.
[33] Kalmikov, A., Dykes, K., and Araujo, K., *Wind Power Fundamentals*, MIT, Cambridge, MA, https://web.mit.edu/windenergy/windweek/Presentations/Wind%20Energy%20101.pdf
[34] King, J., Clifton, A., and Hodge, B. M., 2014, "Validation of Power Output for the WIND Toolkit," National Renewable Energy Laboratory, Report No. NREL/TP-5D00-61714, Golden, CO, https://www.nrel.gov/docs/fy14osti/61714.pdf
[35] Holmgren, W. F., Hansen, C. W., and Mikofski, M. A., 2018, "pvlib Python: A Python Package for Modeling Solar Energy Systems," J. Open Source Softw., **3**(29), p. 884.
[36] Sengupta, M., Xie, Y., Lopez, A., Habte, A., Maclaurin, G., and Shelby, J., 2018, "The National Solar Radiation Data Base (NSRDB)," Renewable Sustainable Energy Rev., **89**, pp. 51–60.
[37] Preger, Y., Barkholtz, H. M., Fresquez, A., Campbell, D. L., Juba, B. W., Romàn-Kustas, J., Ferreira, S. R., and Chalamala, B., 2020, "Degradation of Commercial Lithium-Ion Cells as a Function of Chemistry and Cycling Conditions," J. Electrochem. Soc., **167**(12), p. 120532.
[38] Spotnitz, R., 2003, "Simulation of Capacity Fade in Lithium-Ion Batteries," J. Power Sources, **113**(1), pp. 72–80.